Assessment of the Operational Applicability of RADARSAT-1 Data for Surface Soil Moisture Estimation

Jesús Álvarez-Mozos, Javier Casalí, María González-Audícana, and Niko E. C. Verhoest

***Abstract*—The present paper focuses on the ability of currently available RADARSAT-1 data to estimate surface soil moisture over an agricultural catchment using the theoretical integral equation model (IEM). Five RADARSAT-1 scenes acquired over Navarre (north of Spain) between February 27, 2003 and April 2, 2003 have been processed. Soil moisture was measured at different fields within the catchment. Roughness measurements were collected in order to obtain representative roughness parameters for the different tillage classes. The influence of the cereal crop that covered most of the fields was taken into account using the semiempirical water cloud model. The IEM was run in forward and inverse mode using vegetation corrected RADARSAT-1 data and surface roughness observations. Results showed a great dispersion between IEM simulations and observations at the field scale, leading to inaccurate estimations. As the surface correlation length is the most difficult parameter to measure, different approaches for its estimation have been tested. This analysis revealed that the spatial variability in the surface roughness parameters seems to be the reason for the dispersion observed rather than a deficient measurement of the correlation length. At the catchment scale, IEM simulations were in good agreement with observations. The error values obtained in the inverse simulations were in the range of *in situ* soil moisture measuring methods ($0.04\ \mathrm{cm}^3 \cdot \mathrm{cm}^{-3}$). Taking into account the small size of the catchment studied, these results are encouraging from a hydrological point of view.**

***Index Terms*—Hydrology, integral equation model (IEM), soil moisture retrieval.**

I. Introduction

ACTIVE microwave (radar) remote sensing represents an interesting alternative to classic point-based surface soil moisture (SM) measuring techniques. The dependence of microwave scattering over bare soil surfaces on the dielectric constant of soils allows the extraction of soil moisture information from radar observations [1]. In addition, radar observations cover large areas with a certain periodicity and have a high spatial resolution. These characteristics make radar-based soil moisture estimation very attractive to domains like hydrology, agronomy, and meteorology [2].

Radar-based SM retrieval has been intensively studied in the last decades. Three main approaches have been generally followed [3]: 1) empirical linear regression models relating the backscattering coefficient (σ^0) to SM, which are valid for invariant roughness, vegetation, and scene acquisition conditions [1]; 2) change detection techniques for monitoring SM dynamics, assuming that surface roughness and vegetation cover change more slowly than SM does [2], [4]; 3) electromagnetic scattering models that simulate the surface backscattering process [5], [6]. Apart from those three main approaches, some other techniques have been recently developed based on radar observations acquired on multiple frequencies [7] or multiple incidence angles [8], [9]. The multifrequency approach yields good results [7], but currently there are no multifrequency spaceborne radar sensors available. The approach using radar observation-acquired at multiple incidence angles, is based on the different response of rough surfaces with increasing incidence angles. Although this approach has shown to be valuable [8], [9], it can only be applied if radar observations are available at two different incidence angles with the same soil surface conditions.

The linear regression approach has been widely used, mainly because of its simplicity [10], [11]. However, its empirical nature and its sensitivity to surface roughness, vegetation or scene configuration variations, particularly the incidence angle [3], reduce its applicability. Similarly, the change detection approach requires the surface characteristics apart from SM to remain unchanged and the scene parameters to be exactly the same [12]. If identical scene parameters were needed, the revisit time of most sensors would be on the order of several weeks, which is generally insufficient for most hydrological and agronomic applications. Apart from that, vegetation and surface roughness can change dramatically over short time periods in agricultural areas [3]. Therefore, it would seem that the application of electromagnetic scattering models is the most suitable approach for the estimation of SM for hydrological and agronomic applications over agricultural areas, however, this approach requires additional parameters, such as roughness, for each image acquisition.

Several models have been proposed for bare soil surface conditions: empirical models [13], [14]; theoretical models, such as the integral equation model (IEM) [5], [6]; and semiempirical models [15]–[18]. The estimation of SM over vegetated surfaces is more complicated because the vegetation cover also interferes in the backscattering process. In these cases the appli-

Manuscript received April 15, 2005. This work was supported in part by the Spanish Government's National Scientific Research, Development, and Technological Innovation Plan, project code REN2003-03028/HID, in part by the Canadian Space Agency Data for Research Use program project DRU-10-02, and in part by the U.S. Department of Agriculture under Agreement 58-6408-0-F137. Any opinions, findings, conclusion, or recommendations expressed in this publication are those of the authors and do not necessarily reflect the view of the U.S. Department of Agriculture.

J. Álvarez-Mozos, J. Casalí, and M. González-Audícana are with the Department of Projects and Rural Engineering, Public University of Navarre, 31006 Pamplona, Spain (e-mail: jesus.alvarez@unavarra.es).

N. E. C. Verhoest is with the Laboratory of Hydrology and Water Management, Ghent University, B-9000 Ghent, Belgium.

Digital Object Identifier 10.1109/TGRS.2005.862248

cation of the radiative transfer principles has led to the development of physically based models that, under certain circumstances, could be simplified to semiempirical algorithms such as the water cloud model [19].

Even if empirical backscattering models performed correctly in some cases [8], [20], they are site-dependent and therefore only applicable under the same conditions they were developed for. Theoretical models are thus preferable although they usually require a larger number of parameters, which are sometimes difficult to estimate. At present, the IEM, a theoretical backscattering model with the widest range of applicability, is the one most frequently used for radar-based soil moisture retrieval [3].

However, the application of the IEM to natural conditions frequently yielded poor results. Mostly, the reasons for this malfunctioning could be related to the fact that the mathematical description of the surface roughness used in the model did not correctly represent natural surfaces [8], [21]. In addition, it has been reported that an accurate field measurement of the required roughness parameters, in particular the correlation length l, is extremely difficult to perform [21], [22]; causing the agreement between IEM simulations and radar observations to be scant [23]–[25]. Furthermore, the model seems to be more sensitive to the roughness parameters than to the soil moisture content [26], especially over smooth surfaces and wet conditions [7], causing small inaccuracies in the measurement of the roughness parameters to be translated into erroneous soil moisture retrievals.

The main problems in the estimation of SM through radar data using the IEM seem to be related to the sensitivity of the model to the surface roughness parameters and their characterization. In the case of agricultural surfaces, roughness is primarily related to tillage practices. Therefore, we will investigate whether reference roughness parameters representative of each tillage practice can be used for the retrieval of SM. This would allow assigning one set of roughness parameters to fields with a specific tillage. Such approach would therefore overcome the need of performing roughness measurements simultaneously with each radar image acquisition, especially in the case of winter cereal crops, where after sowing no tillage takes place during the whole growing season. Under these conditions surface roughness can be assumed to be constant.

The main objective of this paper is to assess the feasibility of operational SM estimation through RADARSAT-1 data over agricultural areas based on the inversion of the IEM. Two main issues are addressed: 1) the application of the IEM considering tillage representative surface roughness parameters at the field scale and average roughness parameters at the catchment scale, and 2) the correction of the influence that an early cereal cover exerts on the SM estimation. In the following sections the test site and the RADARSAT-1 data are described as well as the methods applied. Finally, results are discussed and conclusions are drawn.

II. Materials

A. Test Site

The research was carried out over a small agricultural watershed located in the Spanish region of Navarre called La Tejería

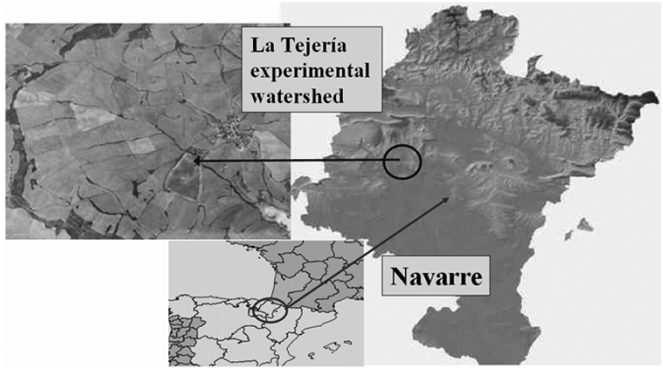

Fig. 1. Location of La Tejería experimental watershed.

(Fig. 1). This watershed is part of the Experimental Agricultural Watershed Network of Navarre, created by the local Government of Navarre in 1993 and aimed at studying the impact of agriculture on the hydrological resources.

The geographical coordinates of the watershed outlet are $42°44'10.6''$N and $1°56'57.2''$W. The watershed covers approximately 160 ha with homogeneous slopes of about 12%, with an altitude ranging from 496–649 m. Its climate is humid submediterranean, with a mean annual temperature of 13 °C. The average annual rainfall is about 700 mm distributed over approximately 105 days.

The watershed has been equipped with an automated meteorological and hydrological station. The station has provided precipitation and flow discharge data on a ten minute basis and daily water quality data (sediment yield, nitrate and phosphate content and other agrochemicals) since 1994.

The most common soils are *Tipic Xerochrepts*, which are less than 1 m deep. Those soils have clayey textures (43% clay, 5% sand, 52% silt) and cover most of the hillslopes. There are also some areas of *Calcixerollic Xerochrepts*, which are slightly deeper (1.0 to 1.5 m) and similar in texture; these appear on the lower parts of the hillslopes. Finally, the valley bottoms are covered with *Fluventic Xerochrept* soils, which are deeper and are silty clay loam in texture (37% clay, 16% sand, 47% silt).

The watershed is almost completely cultivated and the hedgerows and streams are the only areas covered by natural vegetation. During the experimental period, an emerging cereal crop covered most of the fields of La Tejería watershed, except for one Ploughed field and four other fields where vegetable crops had been sown by scattering the seed over previously rolled soils (Fig. 2, Table I). Apart from these fields, some other small ones were covered by bushes and were not considered in the present work. Those cereal fields that had been rolled after sowing and, therefore, had a smoother surface were grouped in a separate crop class called "Rolled cereal." In both cases, the cereal plants were in the 20–30 phenological stage according to the Zadocks scale. Vegetables were very sparse and recently germinated at the beginning of the experimental campaign.

B. Ground Measurements

1) Surface Soil Moisture Measurements: The SM of the top 10 cm of the soil was measured on each image acquisition day

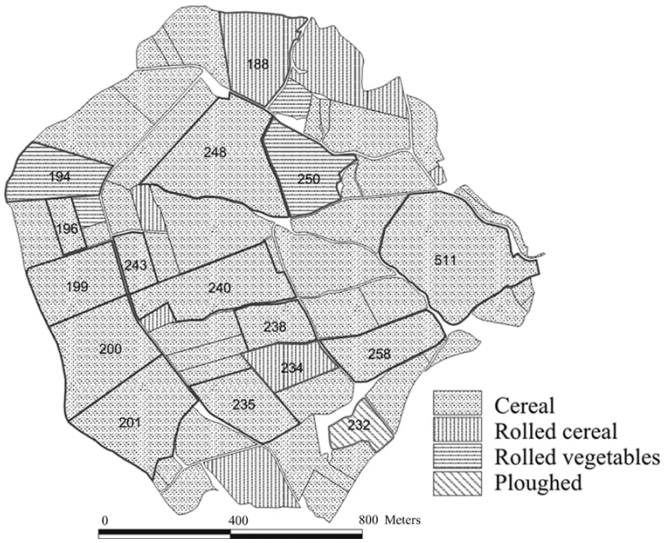

Fig. 2. Spatial distribution of crop classes observed over La Tejería watershed. Monitored control fields appear outlined and numbered.

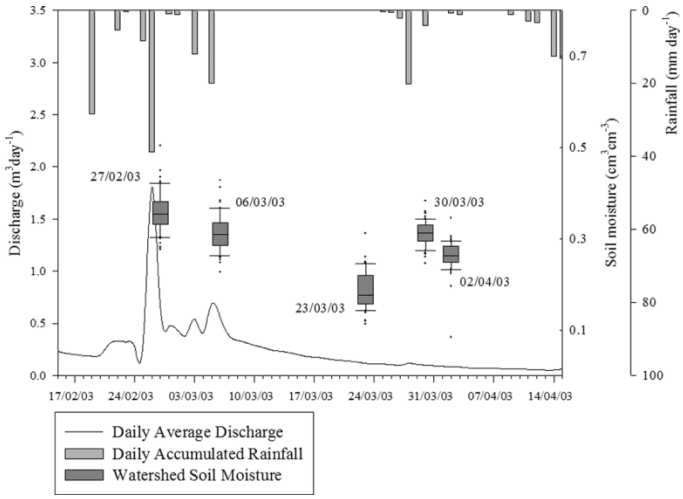

Fig. 3. Ground measured soil moisture (SM) data during the experimental campaign, rainfall distribution (bars) and discharge data (line). Dates are given in dd/mm/yy format.

TABLE I
DESCRIPTION OF CROP CLASSES OBSERVED. THE TOTAL NUMBER OF FIELDS AND AREA OF EACH CLASS IS SHOWN, AS WELL AS THE NUMBER AND AREA OF THE MONITORED FIELDS

Class	Description	No. of fields	Total area (ha)	No. of monitored fields	Total area of monitored fields (ha)
Cereal	Winter cereal conventionally sown	52	126.27	11	59.86
Rolled cereal	Winter cereal rolled after sowing	8	17.95	2	7.90
Rolled vegetables	Chickpeas sown scattered over rolled fields	4	10.35	2	8.58
Ploughed	Ploughed fields with bare soil surface	1	1.77	1	1.77

TABLE II
MEASURED ROUGHNESS PARAMETERS FOR EACH CROP CLASS. THE NUMBER OF COLLECTED PROFILES PER CLASS IS SHOWN (N), AS WELL AS THE AVERAGE AND STANDARD DEVIATION OF THE TWO ROUGHNESS PARAMETERS: s AND l

Class	N	Average s (cm)	Standard deviation s (cm)	Average l (cm)	Standard deviation l (cm)
Rolled vegetables	16	0.474	0.089	2.436	2.836
Rolled cereal	20	0.889	0.268	3.621	3.263
Cereal	48	1.046	0.341	3.492	2.631
Ploughed	4	2.568	0.723	7.410	2.354

using a commercial Time Domain Reflectometry (TDR) instrument (TRIME FM-3, IMKO GmBH) connected to a portable three-rod probe.

SM was sampled following a stratified random sampling scheme along the catchment, in order to obtain accurate catchment SM averages. Sixty sampling points were monitored each day and three TDR measurements were averaged out at each sampling point in order to reduce the small scale SM variability and the probe error. Apart from that, 16 control fields were selected (Fig. 2) where a minimum of three sampling points was measured. The area of those fields ranged from 1.3 (field 196) to 11.1 ha (field 511). Wooding *et al.* [27] found that a minimum field size of 1 ha would give a variability in the estimated backscatter smaller than ± 0.25 dB on ERS-1 scenes, overcoming the effects of the SAR speckle. On the other hand, very large fields can show differentiated in-field SM patterns due to their great spatial variability, complicating the calculation of representative average SM values. Biftu and Gan [28] found that the maximal length over which SM behaved homogeneously is 300 m.

Average catchment SM values were calculated through a weighted mean taking into account the crop and soil classification. The SM values observed reflected rainfall patterns throughout the experimental campaign (Fig. 3).

2) Surface Roughness Measurements: In the present research, surface roughness was measured using a 1-m-long needle profiler with a sampling interval of 2 cm. The accuracy of surface roughness measurements, for SAR applications, has often been related to the length of the profile measuring device [21], [29], suggesting that long profiles (up to 10 m or longer) are needed in order to achieve a reasonable accuracy. However, such measurements are difficult and costly to perform and reduce the applicability of radar remote sensing soil moisture estimation. Davidson *et al.* [30] investigated the validity of 1-m-long surface roughness profiles and proposed a standardized procedure for the utilization of this kind of profile that yielded acceptable results over medium surface roughness conditions.

Profiles were collected parallel and perpendicular to the tillage row direction. According to Ulaby *et al.* [31], the random component of surface roughness that influences the backscattering process should be separated from any periodic pattern, such as a row structure. This periodic patter will also influence the backscattering through the local slope, particularly at high incidence angles and over deeply furrowed fields. In the case of the fields observed the surface was assumed to be isotropic because no clear row pattern was evidenced except for the Ploughed field (field 232). The surfaces observed were assumed to be correctly described as stationary, randomly rough surfaces, characterized through a single spatial scale in both the horizontal and vertical directions. Therefore, the

TABLE III
VALUES OF THE TWO ROUGHNESS PARAMETERS: STANDARD DEVIATION OF SURFACE HEIGHTS (s) AND CORRELATION LENGTH (l), MEASURED BY OTHER AUTHORS OVER DIFFERENT TILLAGE CONDITIONS. TWO VALUES SEPARATED BY "–" INDICATE GIVEN MINIMUM AND MAXIMUM VALUES FOR EACH CLASS, IN OTHERS THE AVERAGE VALUE PLUS/MINUS THE STANDARD DEVIATION OF THE MEASUREMENTS IS GIVEN

Reference	Rolled		Wheat sowing (seedbed)		Rice sowing (seedbed)		Harrowed		Ploughed	
	s (cm)	l (cm)	s (cm)	l (cm)	s (cm)	l (cm)	s (cm)	l (cm)	s (cm)	l (cm)
Rakotoarivony *et al.* [23]	–	–	0.80–1.50	2.30–3.40	–	–	–	–	2.70	8.70
Zribi *et al.* [32]	–	–	0.55–0.92	2.51–12.68	–	–	–	–	0.97-3.77	6.10-8.10
Davidson *et al.* [21]	0.80±0.20	2.70±0.80	1.00±0.30	2.90±0.80	–	–	1.70±0.30	4.40±0.70	3.50±0.60	6.10±1.00
Davidson *et al.* [33]	–	–	–	–	0.64	5.40	–	–	–	–
Bindlish and Barros [7]	–	–	0.56-1.18	–	–	–	–	–	–	–
Davidson *et al.* [30]	–	–	0.60±0.30	3.70±2.60	–	–	1.60±0.70	3.80±2.90	2.70±1.00	6.90±2.70

profiles were processed following the procedure proposed in [30] to extract two classic roughness parameters: s (standard deviation of surface heights) and l (surface correlation length) [1].

Surface roughness was considered to be invariable in time because no tillage was performed in the experiment period and the intensity of the precipitation events observed was low. The autocorrelation functions calculated were closer to the exponential than to the Gaussian function.

In all, 88 profiles were collected over the catchment. The number of profiles acquired per class depended on the number of fields belonging to each class (Table II). The catchment average s and l values were 1.00 and 3.47 cm with standard deviations of 0.13 and 2.87 cm, respectively. The catchment average s value was calculated as the weighted average of the different classes, and the average l value was derived from the average autocorrelation function of the different classes. The roughness parameters per class measured are detailed in Table II and show similar values to those observed in the literature (Table III).

3) Vegetation Cover Measurements: Vegetation parameters were not measured in La Tejería during the experiment period. Instead, crop parameters recorded over a neighboring experimental area and a Landsat-7 ETM+ scene acquired on March 17, 2003 were used to characterize the vegetation cover of the vegetated fields in the catchment (corresponding to the classes "Cereal" and "Rolled cereal"). The neighboring experimental site, located 25 km away from La Tejería, showed a winter cereal crop that was sown on the same dates. The soil conditions and climate were also very similar to those of La Tejería. Vegetation parameters, i.e., vegetation water content (M_V) and leaf area index (LAI), were measured periodically (January 17, March 18, and April 8, 2003) and afterward linearly interpolated for the five image acquisition days (Table IV). Those interpolated values were assumed to be representative of the average conditions of the vegetated fields in La Tejería.

To account for the vegetation cover variability between the different vegetated fields in the catchment, the NDVI, which can be used as a proxy of vegetation biomass [34], was derived from the Landsat-7 ETM+ scene. The scene was processed using classical techniques. First, the image was orthorectified using ground control points and a digital elevation model (DEM). Then, the atmospheric absorption was corrected following the improved dark object subtraction method [35]. Afterward, the reflectivity of the different bands in the image was calculated and the NDVI was obtained. The average NDVI value calculated in the vegetated fields of the catchment was 0.550. This value was assumed to correspond to the estimated vegetation parameters for that date from the neighboring site, i.e., LAI $= 2.772$ and $M_V = 0.940$ kg $\cdot$ m^{-2}. Afterward, the vegetation parameters for each field and date were calculated based on two assumptions: 1) the temporal evolution of the individual fields can be correctly represented by the interpolated average values for each date, and 2) the variability between the different fields during the experiment period can be reflected by the ratio between the NDVI values of each field and the average NDVI value obtained from the Landsat scene. Therefore, the following expression was used to calculate the M_V value of each field and date:

$$\frac{M_{V\,i,j}}{\mathrm{NDVI}_{i,\mathrm{March17}}} = \frac{\overline{M_V}_{\,j}}{\overline{\mathrm{NDVI}}_{\mathrm{March17}}} \tag{1}$$

where $M_{Vi,j}$ is the vegetation moisture content of the field i on the day j, $\mathrm{NDVI}_{i,\mathrm{March17}}$ is the NDVI value of the field i as observed in the Landsat-7 ETM+ scene of the March 17, 2003, $\overline{M_V}_j$ is the average moisture content of the vegetated fields on the day j, and $\overline{\mathrm{NDVI}}_{\mathrm{March17}}$ is the average NDVI of the vegetated fields as observed in the Landsat scene.

The same approach was used to calculate the LAI values for each field and date. Calculated values of M_V and LAI are shown in Table V. Although the validity of the approach used to obtain the vegetation parameters may be debatable, we think that the

TABLE IV
ESTIMATED AVERAGE CEREAL COVER PARAMETERS FOR EACH IMAGE ACQUISITION DATE FROM THE PARAMETERS MEASURED IN A NEIGHBORING EXPERIMENTAL SITE. DATES ARE GIVEN IN dd/mm/yy FORMAT

Date	Days after Sowing	M_V (kg m^{-2})	LAI
27/02/03	127	0.661	2.149
06/03/03	134	0.728	2.267
23/03/03	151	1.056	3.048
30/03/03	158	1.239	3.512
02/04/03	161	1.317	3.711

TABLE V
ESTIMATED CEREAL COVER PARAMETERS FOR EACH CONTROL FIELD AND IMAGE ACQUISITION DATE. CATCHMENT AVERAGE PARAMETERS ARE ALSO SHOWN. DATES ARE GIVEN IN dd/mm/yy FORMAT

Field	Class	27/02/03		06/03/03		23/03/03		30/03/03		02/04/03	
		LAI	M_V (kg m^{-2})	LAI	M_V (kg m^{-2})	LAI	M_V (kg m^{-2})	LAI	M_V (kg m^{-2})	LAI	M_V (kg m^{-2})
188	Rolled cereal	1.868	0.574	1.970	0.633	2.649	0.918	3.052	1.077	3.225	1.145
234	Rolled cereal	2.464	0.758	2.599	0.835	3.495	1.211	4.027	1.421	4.255	1.510
196	Cereal	2.037	0.626	2.148	0.690	2.889	1.001	3.328	1.174	3.517	1.248
199	Cereal	1.527	0.469	1.611	0.517	2.166	0.751	2.495	0.880	2.637	0.936
200	Cereal	1.837	0.565	1.938	0.623	2.606	0.903	3.002	1.059	3.172	1.126
201	Cereal	1.923	0.591	2.028	0.652	2.727	0.945	3.142	1.109	3.320	1.179
235	Cereal	2.519	0.774	2.657	0.854	3.573	1.238	4.117	1.452	4.350	1.544
238	Cereal	2.007	0.617	2.117	0.680	2.847	0.987	3.280	1.157	3.466	1.230
240	Cereal	2.248	0.691	2.371	0.762	3.188	1.105	3.673	1.296	3.881	1.378
243	Cereal	2.326	0.715	2.454	0.788	3.300	1.144	3.802	1.341	4.017	1.426
248	Cereal	1.816	0.558	1.916	0.615	2.576	0.893	2.968	1.047	3.136	1.113
258	Cereal	2.190	0.673	2.310	0.742	3.106	1.076	3.578	1.262	3.781	1.342
511	Cereal	2.290	0.704	2.415	0.776	3.247	1.125	3.742	1.320	3.954	1.403
Catchment Average		2.149	0.661	2.267	0.728	3.048	1.056	3.512	1.239	3.711	1.317

hypotheses assumed did no lead to significant errors as the experiment period was very short (34 days), and the conditions of the neighboring site, regarding crop growth, correctly reflected the conditions of La Tejería catchment. However, we suppose that if the vegetation parameters obtained by these means are used for further calculations there will be a certain level of inaccuracy that needs to be taken into account when interpreting the results.

If two or more optical images were available, one acquired at the beginning of the cereal growing cycle and one at crop maturity, a similar approach could be developed assuming that the NDVI is a good indicator of the vegetation parameters. Such an approach could be useful for evaluating and correcting the attenuation of microwave radiation by cereal canopies in an operational way without needing to perform any ground measurements.

C. Radarsat-1 Scenes

Five RADARSAT-1 SGF scenes were acquired over the Navarre region during spring 2003. RADARSAT-1 offers the possibility of decreasing the revisit time from the standard 24 days cycle to one or two weeks by combining different beam modes and ascending and descending passes. In this case, five scenes were acquired in a period of approximately one month. This fact can be of great interest for the monitoring of rapidly changing terrain variables such as SM. Beam modes S1 and S2 were selected for their lower incidence angles. At low incidence angles vegetation-induced attenuation, as well as surface roughness influence, are minimized, so that those scenes are more appropriate for soil moisture retrieval [1]. Besides, the RADARSAT-1 configuration (C-band and HH polarization), at low incidence angles, has proved to be particularly well suited for SM research over cereal canopies where vertically polarized waves are more intensively attenuated [28], [36]. Table VI shows the main characteristics of the RADARSAT-1 scenes used in this study.

The five RADARSAT-1 SGF scenes were converted from 16-bit gray levels to σ^0 values following the standard approach [37]. The local incidence angle, required for the calculation of σ^0, was computed taking into account the slope and aspect of each pixel [38].

TABLE VI
MAIN CHARACTERISTICS OF RADARSAT-1 SGF SCENES USED

Date dd/mm/yy	Time hh/mm/ss	Pass	Beam mode	Incidence angle (deg)	Resolution range x azimut (m)
27/02/03	06:23:10	DESCENDING	S1	20-27	24 x 27
06/03/03	06:23:02	DESCENDING	S2	24-31	20 x 27
23/03/03	06:23:09	DESCENDING	S1	20-27	24 x 27
30/03/03	06:18:57	DESCENDING	S2	24-31	20 x 27
02/04/03	17:50:22	ASCENDING	S1	20-27	24 x 27

Scenes were geocoded following the standard ground control point approach, maintaining the root mean square error (rmse) below one pixel. Despite being four-look images, the speckle was still apparent, so the images were filtered for speckle reduction using a 7×7 window adaptive Gamma MAP filter [39]. Finally, σ^0 values corresponding to each ground sampling point were calculated and field and catchment average values were computed.

III. METHODOLOGY

A. Correction of the Influence of the Vegetation Cover

The ability of microwaves to penetrate through a vegetation canopy depends on the wavelength, incidence angle and polarization as well as on the characteristics of the vegetation canopy [31]. The IEM was formulated for bare soil conditions, thus its application to vegetated surfaces is only possible in the case of weakly developed canopies that do not interfere in the backscattering process. This is more likely to happen at low incidence angles and long wavelengths [1].

Previous studies reported that a wheat cover 10–15 cm high did not significantly affect the backscattering process at an incidence angle of 23° and C-band [36]. However, in the case of more developed cereal crops the σ^0 can be attenuated by the canopy causing severe discrepancies between IEM simulations and observed σ^0 values. In terms of the NDVI, values higher than 0.1 have been reported to significantly affect σ^0 as observed on ERS-1 data [40]. More recently, a threshold in terms

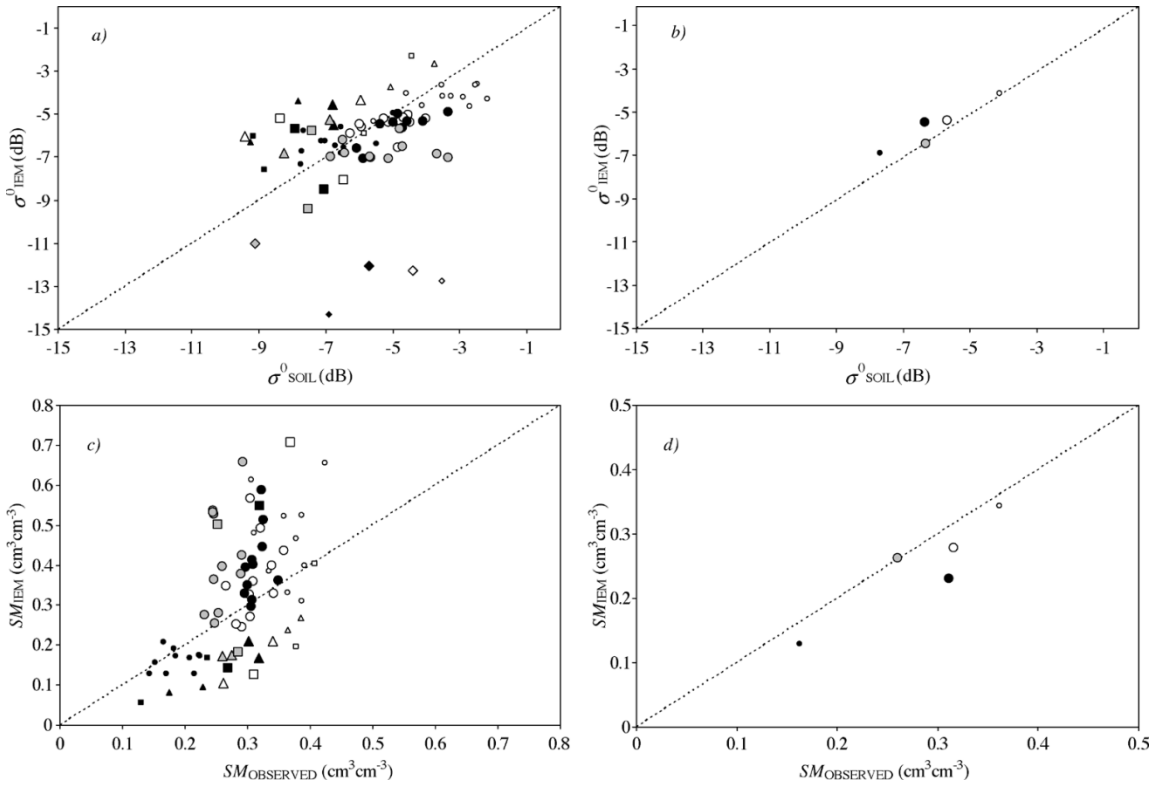

Fig. 4. IEM model simulations plotted against observations. (a) Forward IEM applied at the field scale and (b) at the catchment scale. (c) Inverse IEM applied at the field scale and (d) at the catchment scale. Symbols represent different crop classes and dates as follows. At the field scale, (a) and (c), circles correspond to the class "Cereal." (Small open circle) 27/02/03. (Large open circle) 06/03/03. (Small dark circle) 23/03/03. (Large dark circle) 30/03/03. (Gray circle) 02/04/03. Triangles to the class "Rolled cereal." (Small open triangle) 27/02/03. (Large open triangle) 06/03/03. (Small dark triangle) 23/03/03. (Large dark triangle) 30/03/03. (Gray triangle) 02/04/03. Squares to the class "Rolled vegetables." (Small open square) 27/02/03. (Large open square) 06/03/03. (Small dark square) 23/03/03. (Large dark square) 30/03/03. (Gray square) 02/04/03. Diamonds to the class "Ploughed." (Small open diamond) 27/02/03. (Large open diamond) 06/03/03. (Small dark diamond) 23/03/03. (Large dark diamond) 30/03/03. (Gray diamond) 02/04/03. At the catchment scale, (b) and (d), circles are used representing the different dates as follows. (Small open circle) 27/02/03. (Large open circle) 06/03/03. (Small dark circle) 23/03/03. (Large dark circle) 30/03/03. (Gray circle) 02/04/03.

TABLE VII
ROOT MEAN SQUARE ERROR (rmse) VALUES OBTAINED IN THE IEM SIMULATIONS. σ^0 rmse REFERS TO THE ERRORS OBTAINED IN THE FORWARD MODELING AND SM rmse REFERS TO THE ERRORS OBTAINED IN THE INVERSE MODELING

Class	σ^0 *rmse* (dB)	*SM rmse* (cm^{3}cm^{-3})
Cereal	1.063	0.136
Rolled cereal	2.238	0.121
Rolled vegetables	2.047	0.182
Ploughed	7.003	–
Catchment scale	0.616	0.043

TABLE VIII
GROUND MEASURED SURFACE ROUGHNESS PARAMETERS AND l VALUES CALCULATED FROM (9) AS PROPOSED IN [30]

Class	Measured parameters		Calculated l (cm) after [30]
	s (cm)	l (cm)	
Rolled vegetables	0.474	2.436	2.228
Rolled cereal	0.889	3.621	2.892
Cereal	1.046	3.492	3.144
Ploughed	2.568	7.410	5.579
Catchment average	1.002	3.466	3.075

of canopy moisture content (M_V) of 0.5 kg $\cdot$ m^{-2} has been proposed for an estimation of SM based on C-band radar data without taking into account the vegetation influence [41].

In the present research, even if the cereal canopy of the vegetated fields was at early development stages, the estimated MV values (Table V) and NDVI observations suggested that the vegetation cover could influence the backscattering response particularly at the end of the experiment period. Therefore, a semiempirical approach, based on the water cloud model [20], was followed in order to correct the σ^0 observations over vegetated fields for the influence of the canopy [3].

The water cloud model represents the canopy as a cloud of identical discrete scatterers that attenuates the microwave radiation and also contributes to the total canopy backscatter as shown in

$$\sigma^0_{\text{can}} = \sigma^0_{\text{veg}}(\theta_{\text{inc}}) + \frac{\sigma^0_{\text{soil}}(\theta_{\text{inc}})}{L^2(\theta_{\text{inc}})} \tag{2}$$

where σ^0_{can} is the total backscattering coefficient observed from the canopy in square meters per square meter (m^2 $\cdot$ m^{-2}), $\sigma^0_{\text{veg}}(\theta_{\text{inc}})$ is the vegetation contribution to the total backscattering depending on the incidence angle, and $\sigma^0_{\text{soil}}(\theta_{\text{inc}})$ is the contribution of the soil that is attenuated twice by the canopy through its loss factor $L(\theta_{\text{inc}})$.

Because in our study, the canopy is at an early development stage, $\sigma^0_{\text{veg}}(\theta_{\text{inc}})$ was considered to be negligible, assuming that the canopy only influenced the backscattering by attenuating the

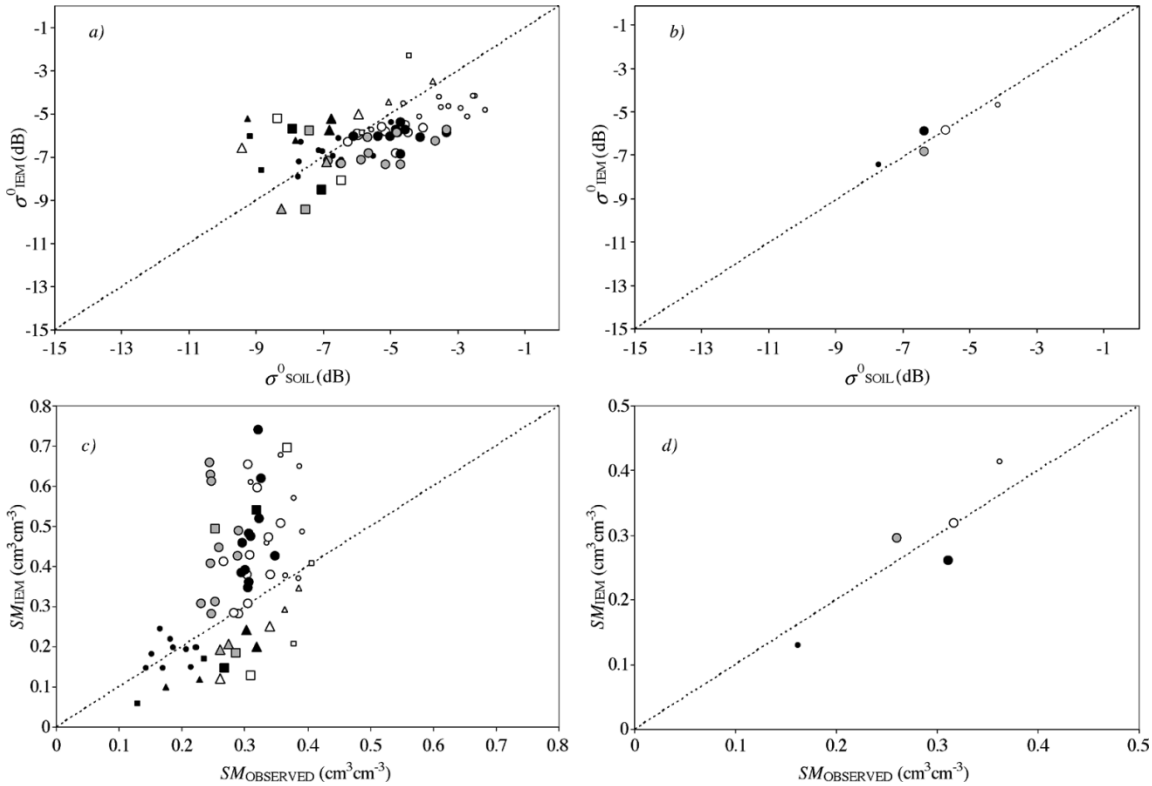

Fig. 5. IEM model simulations plotted against observations. Surface correlation length (l) values used in these simulations are obtained after (9). (a) Forward IEM applied at the field scale and (b) at the catchment scale. (c) Inverse IEM applied at the field scale and (d) at the catchment scale. Symbols represent different crop classes and dates as in Fig. 4.

TABLE IX
ROOT MEAN SQUARE ERROR (rmse) VALUES OBTAINED IN THE IEM SIMULATIONS. σ^0 rmse REFERS TO THE ERRORS OBTAINED IN THE FORWARD MODELING AND SM rmse REFERS TO THE ERRORS OBTAINED IN THE INVERSE MODELING. l VALUES CALCULATED FROM (9) WERE USED

Class	σ^0 *rmse* (dB)	*SM rmse* (cm^{3}cm^{-3})
Cereal	1.334	0.179
Rolled cereal	1.641	0.089
Rolled vegetables	1.966	0.176
Ploughed	–	–
Catchment scale	0.400	0.036

radiation [42]. The vegetation loss factor can be presumed to depend solely on M_V and the incidence angle as

$$L(\theta_{\text{inc}}) = \exp\left(\frac{B_1 M_V}{\cos\theta_{\text{inc}}}\right) \tag{3}$$

where B_1 is an empirical constant. Shifting to decibel units and assuming that $\sigma^0_{\text{soil}}(\theta_{\text{inc}})$ depends linearly on SM, (4) is obtained

$$\sigma^0_{\text{can}} = \frac{-20B_1}{\ln 10 \cdot \cos\theta_{\text{inc}}} M_V + C \cdot \text{SM} + D. \tag{4}$$

Once the water cloud model is fitted, the backscattering values observed can be corrected by subtracting the vegetation attenuation component from the following canopy backscattering coefficient, leading to a backscattering coefficient for a bare soil surface as proposed in Taconet *et al.* [42]:

$$\sigma^0_{\text{soil}} = \sigma^0_{\text{can}} - \frac{-20B_1}{\ln 10 \cdot \cos\theta_{\text{inc}}} M_V. \tag{5}$$

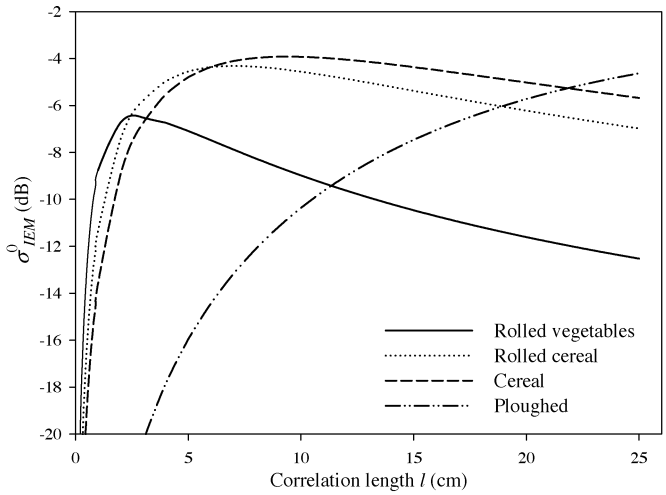

Fig. 6. Sensitivity of the backscattering coefficient σ^0 to the surface correlation length l at each class, according to the IEM model. The following acquisition parameters have been used: C-band (5.3 GHz), HH polarization, and 20° incidence angle. The surface soil moisture has been set to 0.25 cm$^3 \cdot$ cm^{-3}, and the surface roughness correlation function has been assumed to be exponential. Measured s values have been used for each class (Table II).

B. Integral Equation Model [5], [6]

In the present research, a simplified version of the IEM was applied which considers only the single-scattering term of the backscattered wave [26]. This version is applicable to surfaces with small to moderate roughness conditions or at low to medium frequencies. The validity condition for this approximation can be expressed by $ks < 3$ and $m < 0.4$ with

k the wavenumber and m the surface roughness slope, which for exponentially autocorrelated surfaces equals s/l.

The IEM calculates the backscattering coefficient from a surface given its roughness parameters (s, l), its dielectric constant (ε), and the scene acquisition parameters: frequency, incidence angle, and polarization. In the present research, ε was calculated through the dielectric mixing model [43] using SM, soil texture, and temperature data. For the formulation of the IEM version used in this paper, we refer to previous publications [26], [28].

From the hydrological point of view, it is more interesting to invert the IEM for the dielectric constant given the observed σ^0 value, the surface roughness and the scene acquisition parameters. In this paper the inversion is performed through a Newton–Raphson iterative scheme.

IV. Results

A. Correction of the Influence of the Vegetation Cover

As explained above, the influence of the vegetation cover on the σ^0 needs to be taken into account. The semiempirical water cloud model was fitted at the catchment scale (6) and at the field scale to fields corresponding to vegetated classes. Under different surface roughness conditions, the model (4) was fitted separately to each cereal class, yielding (7) in the case of "Cereal" fields and (8) in the case of "Rolled cereal" fields. The backscattering values observed were corrected solving the following:

$$\sigma^0_{\text{can}} = \frac{-1.364 M_V}{\cos\theta_{\text{inc}}} + 0.161 \cdot \text{SM} - 10.329 \qquad R^2 = 0.926 \tag{6}$$

$$\sigma^0_{\text{can}} = \frac{-1.754 M_V}{\cos\theta_{\text{inc}}} + 0.160 \cdot \text{SM} - 9.691 \qquad R^2 = 0.682 \tag{7}$$

$$\sigma^0_{\text{can}} = \frac{-0.764 M_V}{\cos\theta_{\text{inc}}} + 0.252 \cdot \text{SM} - 14.367 \qquad R^2 = 0.836. \tag{8}$$

B. IEM Simulations

The IEM was applied at the field and catchment scale. It was run in its forward mode obtaining σ^0 estimates from surface parameters [Fig. 4(a) and (b)]. Afterward, the inverse algorithm was applied yielding SM values [Fig. 4(c) and (d)]. Results were evaluated in terms of the root mean square error (rmse) between estimated and observed σ^0 values in decibels, and, in the case of inverse modeling, in volumetric SM units, cubic meters per cubic meter ($\text{cm}^3 \cdot \text{cm}^{-3}$) (Table VII).

In general, results show a significant agreement between IEM estimates and observations at the catchment scale, with error values of 0.616 dB or 0.043 $\text{cm}^3 \cdot \text{cm}^{-3}$. However, at the field scale, errors were much higher and no accurate estimations were achieved. The field corresponding to the class "Ploughed" showed no correlation between simulations and observations; moreover, the inverse model could not be solved. This behavior can be explained by the difficulties encountered for adequately measuring the surface soil moisture content on such a rough surface and the great variability of the roughness parameters measured (Table II).

TABLE X
Calibrated Correlation Length Values. The Average Value and Standard Deviation for Each Class Are Shown. Except for the Case of the "Ploughed" Class, Two Calibrated Values Were Obtained for Each Class l_{cal1} and l_{cal2}

Class	l_{cal1} (cm)	Standard deviation l_{cal1} (cm)	l_{cal2} (cm)	Standard deviation l_{cal2} (cm)
Rolled vegetables	1.076	0.279	12.246	6.621
Rolled cereal	1.880	0.361	31.102	14.818
Cereal	3.635	0.852	32.206	18.952
Ploughed	17.162	5.197	–	–
Catchment average	2.787	0.306	29.892	12.855

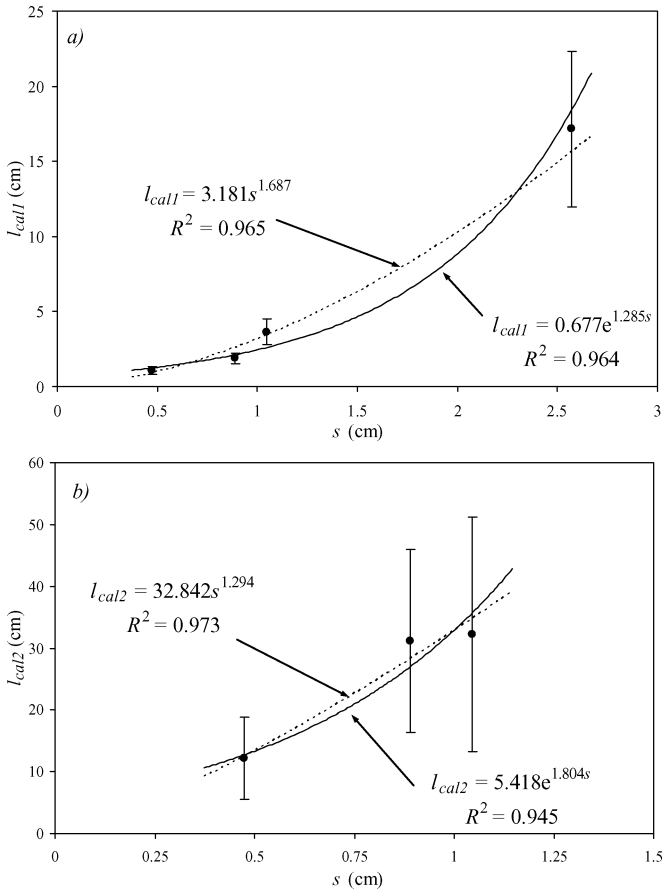

Fig. 7. Relation between s measurements and calibrated l values for each class. (a) shows l_{cal1} values, and (b) shows l_{cal2} values. The error bars represent the standard deviation of the average l value. Two curves have been fitted: exponential (continuous line) according to Baghdadi *et al.* [24] and power (dotted line) according to Baghdadi *et al.* [25].

Apart from that, it must be noted that due to the reduced sensitivity of σ^0 to the dielectric constant in wet conditions, a small error in the σ^0 estimate is translated into a much higher SM error in wet soils than in drier ones, leading to an overestimation of the SM content in wet conditions [Fig. 4(c)].

The cause of the inaccuracy observed at the field scale can be partly due to a deficient measurement of the surface roughness parameters, in particular the surface correlation length (l). Other researchers have outlined the difficulties of adequately measuring l [24]–[26], [30]. Moreover, the characteristics of the profiler used in this experiment period are not those most suitable for an accurate measurement of l.

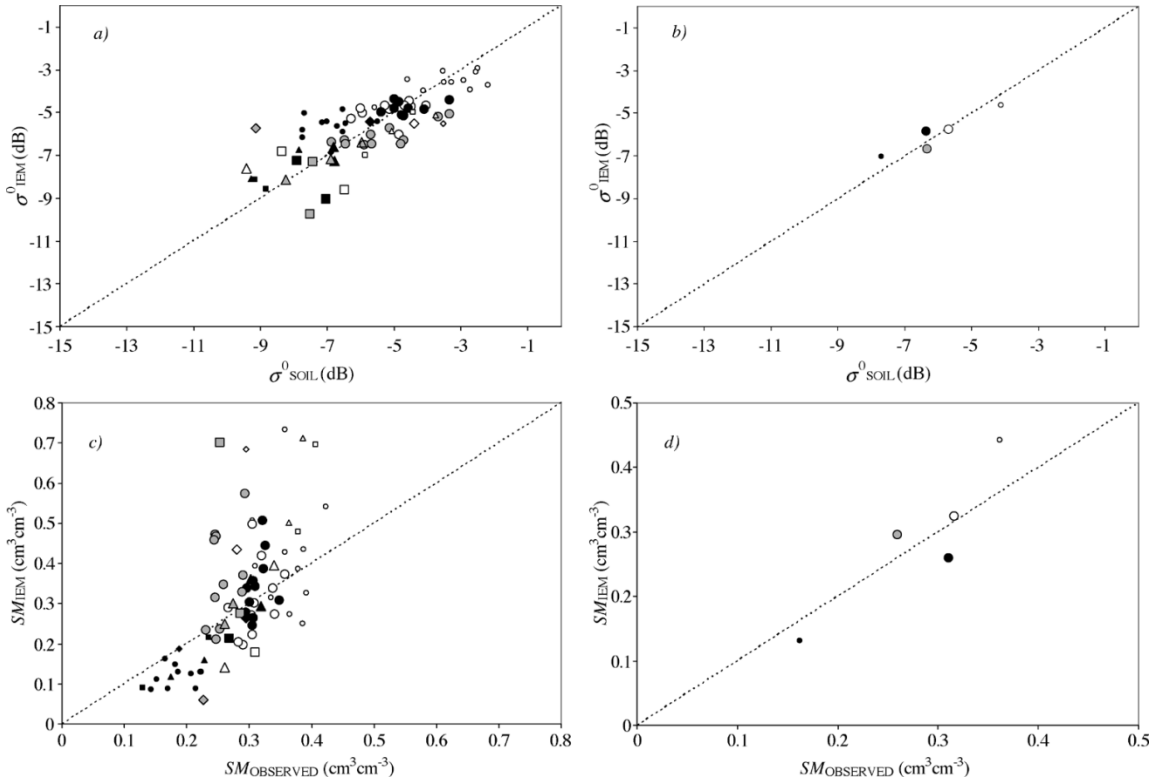

Fig. 8. IEM model simulations plotted against observations. Surface correlation length (l) values used in these simulations correspond to class average l_{cal1} values. (a) Forward IEM applied at the field scale and (b) at the catchment scale. (c) Inverse IEM applied at the field scale and (d) at the catchment scale. Symbols represent different crop classes and dates as in Fig. 4.

Some recent studies focused on the possibility of obtaining l estimates from s values that are easier to measure accurately [24], [25], [30]. For instance, Davidson *et al.* [30] discussed the joint statistical properties of parameters s and l. They observed a linear relation between both parameters that was significant for a wide range of roughness conditions over agricultural surfaces

$$l = 1.47 + 1.6s. \tag{9}$$

Such a relation can be a valuable tool to translate s estimates, which are relatively easy to obtain from a limited set of profile data, into corresponding l values [30].

On the other hand, Baghdadi *et al.* [24] performed an empirical calibration of the parameter l from a set of radar observations and soil parameter measurements, and observed an exponential relationship between the calibrated l values and the s measurements for each radar configuration. In a more recent publication, Baghdadi *et al.* [25] extended their study to observations in different sensor configurations showing that the calibrated l parameter depended not only on s but also on the acquisition parameters.

In the present research both approaches have been tested in order to obtain more accurate l values for each roughness class. First, l values calculated with (9) (Table VIII) were used as input for the next IEM simulations. In this case, the results improved slightly compared to those obtained with ground measured l values, except for the fields corresponding to the class "Cereal" (Fig. 5 and Table IX). However, when using this $s-l$ relationship, the "Ploughed" field fell outside the IEM validity range ($m > 0.4$). At the catchment scale, results also improved slightly from an rmse of 0.043 cm$^3 \cdot$ cm^{-3} to 0.036 cm$^3 \cdot$ cm^{-3}.

In order to test the approach proposed by Baghdadi *et al.* [24], [25], the IEM was solved for l based on σ^0_{soil} observations and SM and s measurements through a Newton–Raphson scheme. Depending on the surface characteristics and the sensor configuration, the IEM can lead to two valid l values for a given σ^0_{soil} observation, this behavior was observed in all the fields of La Tejería apart for the "Ploughed" one (Fig. 6). Calibrated l values were obtained for each roughness class and acquisition date. Average values were computed from the calibrated l values for the five acquisitions. A catchment average calibrated l value was also calculated. These average values and their standard deviations are given in Table X. As mentioned before, for some classes two solutions have been found, referred to as l_{cal1} and l_{cal2} for respectively the lowest and highest value of the calibrated correlation length. The variability observed in the calibrated l values may be a consequence of the radiometric resolution of the sensor and may also reflect the spatial variability between the roughness conditions of fields belonging to each class.

The calibrated l_{cal1} values and their respective s measurements show a clear exponential or power-like relationship [Fig. 7(a)], similar to the results observed by Baghdadi *et al.* [24], [25]. Further observations are needed to confirm this relationship and its dependence on the sensor configuration.

The results obtained using l_{cal1} values were similar to those obtained using l measurements (Fig. 8 and Table XI). At the field scale results improved slightly for the class "Cereal" and increased for the class "Rolled vegetables. " Results improved significantly for the "Ploughed" field although error values were

TABLE XI
ROOT MEAN SQUARE ERROR (rmse) VALUES OBTAINED IN THE IEM SIMULATIONS. σ^0 rmse REFERS TO THE ERRORS OBTAINED IN THE FORWARD MODELING AND SM rmse REFERS TO THE ERRORS OBTAINED IN THE INVERSE MODELING. l_{cal1} VALUES WERE USED IN THE SIMULATION

Class	σ^0 *rmse* (dB)	*SM rmse* (cm^3cm^{-3})
Cereal	1.317	0.112
Rolled cereal	0.950	0.125
Rolled vegetables	1.387	0.248
Ploughed	1.826	0.202
Catchment scale	0.462	0.048

TABLE XII
ROOT MEAN SQUARE ERROR (rmse) VALUES OBTAINED IN THE IEM SIMULATIONS. σ^0 rmse REFERS TO THE ERRORS OBTAINED IN THE FORWARD MODELING AND SM rmse REFERS TO THE ERRORS OBTAINED IN THE INVERSE MODELING. l_{cal2} VALUES WERE USED IN THE SIMULATION

Class	σ^0 *rmse* (dB)	*SM rmse* (cm^3cm^{-3})
Cereal	2.352	0.528
Rolled cereal	1.614	0.288
Rolled vegetables	3.391	0.236
Ploughed	–	–
Catchment scale	1.406	0.208

still high (Table XI). At the catchment scale the SM estimation error increased slightly to a value of 0.048 $cm^3 \cdot cm^{-3}$.

On the other hand, results obtained using l_{cal2} values were significantly worse (Table XII). This is a consequence of the increased difficulty in the inversion of l_{cal2} due to the small slope of the $\sigma^0(l)$ relationship at high l values (Fig. 6). This difficulty is clearly reflected in the high standard deviations of the class average l_{cal2} values obtained (Table X); small inaccuracies in the σ^0 observations result in high errors in the l_{cal2} inversion.

It can be observed that the main reason for the dispersion observed at the field scale is not an deficient field measurement of surface roughness, except for the "Ploughed" class, where the calibrated l_{cal1} value was significantly different from the measured l. The dispersion can be attributed rather to the variability of surface roughness parameters between fields belonging to a same class that in this study was considered as being homogeneous. The high standard deviation of surface roughness measurements at each roughness class (Table II), can result in very different SM estimations because of the great sensitivity of the σ^0 to those roughness parameters, in particular s [7]. It thus seems difficult to obtain accurate roughness parameters representative of a tillage class due to their great spatial variability and their influence on the backscattering process.

Apart from that, the reduced sensitivity of σ^0 to the dielectric constant in wet conditions leads to an overestimation of the SM, sometimes resulting in unrealistic SM values (i.e., values higher than 0.5 $cm^3 \cdot cm^{-3}$). In these cases, a simple interpretation of the results can partially solve the problem assigning a maximum (saturated) SM value to those fields yielding values above saturation.

In conclusion, the strong influence of the surface roughness conditions on the scattering process and their variability makes it difficult to obtain accurate SM estimates from RADARSAT-1 data at the field scale. However, at the catchment scale, the influence of the roughness variability seems to be reduced yielding encouraging results.

V. CONCLUSION

The present research addressed the issue of the operational ability of RADARSAT-1-based surface soil moisture estimation (SM). At the field scale, the results obtained highlight the need of accurate surface roughness measurements in order to adequately estimate SM. The great spatial variability of the surface roughness and the sensitivity of the backscattering coefficient to the roughness parameters make it difficult to obtain roughness parameters representative of a tillage class.

At the field scale, an elevated dispersion between IEM simulations and observations was evidenced, leading to high error values. The main reason for the dispersion observed seems to be related to the spatial variability of the surface roughness parameters, particularly l. This great variability makes it difficult to obtain roughness measurements representative of a certain tillage class, especially over smooth surface conditions. Therefore, if accurate radar-based SM estimations are needed very detailed roughness measurements are required, which reduces the applicability of this approach in an operational manner.

At the catchment scale however, IEM simulations were in good agreement with observations. The error values obtained in the inverse simulations were in the range of *in situ* SM measuring methods (0.04 $cm^3 \cdot cm^{-3}$). Taking into account the small size of the experimental catchment studied in this research (160 ha) these results are encouraging from a hydrological point of view.

It must be pointed out that catchment average soil moisture estimations can be very helpful when applying hydrological models. These values can, for instance, be used for the determination of the antecedent moisture content in runoff-discharge models [44], for the calibration of the catchment hydraulic parameters [45] or for improving the performance of hydrological models and land atmosphere transfer schemes through data assimilation techniques [46], [47].

REFERENCES

[1] F. T. Ulaby, R. K. Moore, and A. K. Fung, *Microwave Remote Sensing, Active and Passive*. Norwood: Artech House, 1982, vol. 1, Radar Remote Sensing: Fundamentals and Radiometry.
[2] E. T. Engman, "Applications of microwave remote sensing of soil moisture for water resources and agriculture," *Remote Sens. Environ.*, vol. 35, no. 2–3, pp. 213–226, 1991.
[3] M. S. Moran, C. D. Peters-Lidard, J. M. Watts, and S. McElroy, "Estimating soil moisture at the watershed scale with satellite-based radar and land surface models," *Can. J. Remote Sens.*, vol. 30, no. 5, pp. 805–826, 2004.
[4] N. E. C. Verhoest, P. A. Troch, C. Paniconi, and F. P. De Troch, "Mapping basing scale variable source areas from multitemporal remotely sensed observations of soil moisture behavior," *Water Resour. Res.*, vol. 34, no. 12, pp. 3235–3244, 1998.
[5] A. K. Fung, Z. Li, and K. S. Chen, "Backscattering from a randomly rough dielectric surface," *IEEE Trans. Geosci. Remote Sens*, vol. 30, no. 2, pp. 356–369, Mar. 1992.
[6] A. K. Fung, *Microwave Scattering and Emission Models and their Applications*. Norwood, MA: Artech House, 1994.
[7] R. Bindlish and A. P. Barros, "Multifrequency soil moisture inversion from SAR measurements using IEM," *Remote Sens. Environ.*, vol. 71, no. 1, pp. 67–88, 2000.

[8] M. Zribi and M. Dechambre, "A new empirical model to retrieve soil moisture and roughness from C-band radar data," *Remote Sens. Environ.*, vol. 84, pp. 42–52, 2002.
[9] N. Baghdadi, S. Gaultier, and C. King, "Retrieving surface roughness parameters and soil moisture from synthetic aperture radar (SAR) data using neural networks," *Can. J. Remote Sens.*, vol. 28, no. 5, pp. 701–711, 2002.
[10] M. Rombach and W. Mauser, "Multi-annual analysis of ERS surface soil moisture measurements of different land uses," in *Proc. 3rd ERS Symp.: Space at the Service of Our Environment*, 1997, pp. 27–34.
[11] A. Quesney, S. Le Hégarat-Mascle, O. Taconet, D. Vidal-Madjar, J. P. Wigneron, C. Loumagne, and M. Normand, "Estimation of watershed soil moisture index from ERS/SAR data," *Remote Sens. Environ.*, vol. 72, no. 3, pp. 290–303, 2000.
[12] E. J. M. Rignot and J. J. van Zyl, "Change detection techniques for ERS-1 SAR data," *IEEE Trans. Geosci. Remote Sens*, vol. 31, no. 4, pp. 896–906, Jul. 1993.
[13] Y. Oh, K. Sarabandi, and F. T. Ulaby, "An empirical model and an inversion technique for radar scattering from bare soil surfaces," *IEEE Trans. Geosci. Remote Sens*, vol. 30, no. 2, pp. 370–381, Mar. 1992.
[14] P. C. Dubois, J. van Zyl, and E. T. Engman, "Measuring soil moisture with imaging radars," *IEEE Trans. Geosci. Remote Sens*, vol. 33, no. 4, pp. 915–926, Jul. 1995.
[15] K. S. Chen, S. K. Yen, and W. P. Huang, "A simple model for retrieving bare soil moisture from radar scattering coefficients," *Remote Sens. Environ.*, vol. 54, no. 2, pp. 121–126, 1995.
[16] J. Shi, J. Wang, A. Y. Hsu, P. E. O'Neill, and E. T. Engman, "Estimation of bare surface soil moisture and surface roughness parameter using L-band SAR image data," *IEEE Trans. Geosci. Remote Sens*, vol. 35, no. 5, pp. 1254–1266, Sep. 1997.
[17] Y. Oh, K. Sarabandi, and F. T. Ulaby, "Semi-empirical model of the ensemble-averaged differential Mueller matrix for microwave backscattering from bare soil surfaces," *IEEE Trans. Geosci. Remote Sens*, vol. 40, no. 6, pp. 1348–1355, Jun. 2002.
[18] Y. Oh, "Quantitative retrieval of soil moisture content and surface roughness from multipolarized radar observations of bare soil surfaces," *IEEE Trans. Geosci. Remote Sens*, vol. 42, no. 3, pp. 596–601, Mar. 2004.
[19] E. W. P. Attema and F. T. Ulaby, "Vegetation modeled as a water cloud," *Radio Sci.*, vol. 13, no. 2, pp. 357–364, 1978.
[20] J. R. Wang, A. Hsu, J. C. Shi, P. E. O'Neill, and E. T. Engman, "A comparison of soil moisture retrieval models using SIR-C measurements over the Little Washita river watershed," *Remote Sens. Environ.*, vol. 59, no. 2, pp. 308–320, 1997.
[21] M. W. J. Davidson, T. Le Toan, F. Mattia, G. Satalino, T. Manninen, and M. Borgeaud, "On the characterization of agricultural soil roughness for radar remote sensing studies," *IEEE Trans. Geosci. Remote Sens.*, vol. 38, no. 2, pp. 630–640, Mar. 2000.
[22] Y. Oh and Y. C. Kay, "Condition for precise measurement of soil surface roughness," *IEEE Trans. Geosci. Remote Sens*, vol. 36, no. 2, pp. 691–695, Mar. 1998.
[23] L. Rakotoarivony, O. Taconet, D. Vidal-Madjar, and M. Benallegue, "Radar backscattering over agricultural bare soils," *J. Electromagn. Waves Appl.*, vol. 10, no. 2, pp. 187–211, 1996.
[24] N. Baghdadi, C. King, A. Chanzy, and J. P. Vigneron, "An empirical calibration of IEM model based on SAR data and measurements of soil moisture and surface roughness over bare soils," *Int. J. Remote Sens.*, vol. 23, no. 20, pp. 4325–4340, 2002.
[25] N. Baghdadi, I. Gherboudj, M. Zribi, M. Sahebi, C. King, and F. Bonn, "Semi-empirical calibration of the IEM backscattering model using radar images and moisture and roughness field measurements," *Int. J. Remote Sens.*, vol. 25, no. 18, pp. 3593–3623, 2004.
[26] E. Altese, O. Bolognani, M. Mancini, and P. A. Troch, "Retrieving soil moisture over bare soil from ERS-1 synthetic aperture radar data: Sensitivity analysis based on a theoretical surface scattering model and field data," *Water Resour. Res.*, vol. 32, no. 3, pp. 653–661, 1996.
[27] M. G. Wooding, G. H. Griffiths, R. Evans, P. Bird, D. Kenward, and G. E. Keyte, "Temporal monitoring of soil moisture using ERS-1 SAR data," in *Proc. 1st ERS-1 Symp.: Space at the Service of Our Environment*, 1993, pp. 641–648.
[28] G. F. Biftu and T. Y. Gan, "Retrieving soil moisture from Radarsat SAR data," *Water Resour. Res.*, vol. 35, no. 5, pp. 1569–1579, 1999.
[29] M. Callens, N. E. C. Verhoest, and M. W. J. Davidson, "Parameterization of tillage-induced single-scale soil roughness from 4-m profiles," *IEEE Trans. Geosci. Remote Sens*, vol. 44, no. 4, pp. 878–888, Apr. 2006.
[30] M. W. J. Davidson, F. Mattia, G. Satalino, N. E. C. Verhoest, T. Le Toan, M. Borgeaud, J. M. B. Louis, and E. Attema, "Joint statistical properties of RMS height and correlation length derived from multisite 1-m roughness measurements," *IEEE Trans. Geosci. Remote Sens.*, vol. 41, no. 7, pp. 1651–1658, Jul. 2003.
[31] F. T. Ulaby, R. K. Moore, and A. K. Fung, *Microwave Remote Sensing, Active and Passive*. Norwood, MA: Artech House, 1986, vol. 3, , From Theory to Applications.
[32] M. Zribi, O. Taconet, S. Le Hegarat-Mascle, D. Vidal-Madjar, C. Emblanch, C. Loumagne, and M. Normand, "Backscattering behavior and simulation comparison over bare soils using SIR-C/X-SAR and ERASME 1994 data over Orgeval," *Remote Sens. Environ.*, vol. 59, no. 2, pp. 256–266, 1997.
[33] M. W. J. Davidson, T. Le Toan, F. Mattia, G. Satalino, and S. Kaojarern, "Using single-parameter SAR data," presented at the *ERS-Envisat Symp.*, Gothemburg, Sweden, 2000.
[34] R. Bindlish and A. P. Barros, "Parameterization of vegetation backscatter in radar-based soil moisture estimation," *Remote Sens. Environ.*, vol. 76, no. 1, pp. 130–137, 2001.
[35] P. S. Chavez, "An improved dark-object subtraction technique for atmospheric scattering correction of multispectral data," *Remote Sens. Environ.*, vol. 24, no. 3, pp. 459–479, 1988.
[36] F. Mattia, T. Le Toan, G. Picard, F. I. Posa, A. D'Alessio, C. Notarnicola, A. M. Gatti, M. Rinaldi, G. Satalino, and G. Pasquariello, "Multitemporal C-band radar measurements on wheat fields," *IEEE Trans. Geosci. Remote Sens.*, vol. 41, no. 7, pp. 1551–1558, Jul. 2003.
[37] N. Shepherd, "Extraction of beta nought and sigma nought from RADARSAT CDPF products," Altrix Systems, Ottawa, ON, Canada, Tech. Rep., 2000.
[38] L. Ulander, "Radiometric slope correction of synthetic aperture radar images," *IEEE Trans. Geosci. Remote Sens.*, vol. 34, no. 5, pp. 1115–1122, Sep. 1996.
[39] A. Lopes, R. Touzi, and E. Nezry, "Adaptive speckle filters and scene heterogeneity," *IEEE Trans. Geosci. Remote Sens.*, vol. 28, no. 6, pp. 992–1000, Nov. 1990.
[40] P. J. van Oevelen and D. H. Hoekman, "Radar backscatter inversion techniques for estimation of surface soil moisture: EFEDA-Spain and HAPEX-Sahel case studies," *IEEE Trans. Geosci. Remote Sens.*, vol. 37, no. 1, pp. 113–123, Jan. 1991.
[41] D. Entekhabi, E. G. Njoku, P. Houser, M. Spencer, T. Doiron, Y. Kim, Y. Smith, R. Girard, S. Belair, W. Crow, T. J. Jackson, Y. H. Kerr, J. S. Kimball, R. Koster, K. C. McDonald, P. E. O'Neill, T. Pultz, S. W. Running, J. Shi, E. Wood, and J. van Zyl, "The Hydrosphere State (Hydros) satellite mission: An Earth system pathfinder for global mapping of soil moisture and land freeze/thaw," *IEEE Trans. Geosci. Remote Sens*, vol. 42, no. 10, pp. 2184–2194, Oct. 2004.
[42] O. Taconet, D. Vidal-Madjar, C. Emblanch, and M. Normand, "Taking into account vegetation effects to estimate soil moisture from C-band radar measurements," *Remote Sens. Environ.*, vol. 56, pp. 52–56, 1996.
[43] C. Dobson, F. T. Ulaby, M. T. Hallikainen, and M. A. El-Rayes, "Microwave dielectric behavior of wet soil, Part II: Dielectric mixing models," *IEEE Trans. Geosci. Remote Sens*, vol. 23, no. 1, pp. GE-35–46, Jan. 1985.
[44] J. M. Jacobs, D. A. Myers, and B. M. Whitfield, "Improved rainfall runoff estimates using remotely sensed soil moisture," *J. Amer. Water. Resour. Assoc.*, vol. 39, no. 2, pp. 313–324, 2003.
[45] E. J. Burke, R. J. Gurney, L. P. Simmonds, and P. E. O'Neill, "Using a modeling approach to predict soil hydraulic properties from passive microwave measurements," *IEEE Trans. Geosci. Remote Sens.*, vol. 36, no. 3, pp. 454–462, Mar. 1998.
[46] V. R. N. Pauwels, R. Hoeben, N. E. C. Verhoest, and F. P. De Troch, "The importance of the spatial patterns of remotely sensed soil moisture in the improvement of discharge predictions for small-scale basins through data assimilation," *J. Hydrol.*, vol. 251, no. 1–2, pp. 88–102, 2001.
[47] V. R. N. Pauwels, R. Hoeben, N. E. C. Verhoest, F. P. De Troch, and P. A. Troch, "Improvement of TOPLATS-based discharge predictions through assimilation of ERS-based remotely sensed soil moisture values," *Hydrol. Process.*, vol. 16, pp. 995–1013, 2002.

Jesús Álvarez-Mozos received the engineering and Ph.D. degrees in agricultural engineering from the Public University of Navarre, Pamplona, Spain, in 2001 and 2006 respectively, with a thesis on radar-based soil moisture retrieval.

Since 2001, he has been an Assistant Professor at the Department of Projects and Rural Engineering, Public University of Navarre. His research interests include remote sensing data processing and hydrological applications of remote sensing.

Javier Casalí received the degree in agricultural engineering from the Polytechnic University of Catalonia, Lleida, Spain, and the Ph.D. degree in agricultural engineering, with a thesis on soil erosion modeling, from the Public University of Navarre, Pamplona, Spain, in 1992 and 1997, respectively.

Since 1999, he has been a Lecturer at the Department of Projects and Rural Engineering, Public University of Navarre, where he is currently involved in research activities on hydrology and soil erosion, and the application of remote sensing to those disciplines.

María González-Audícana received the B.S. and Ph.D. degrees in agricultural engineering, with a thesis based on image-fusion, from the Public University of Navarre, Pamplona, Spain, in 1996 and 2001, respectively.

Since 1997, she has been an Assistant Professor with the Department of Projects and Rural Engineering, Public University of Navarre, where she is currently involved in research activities on multisensor data fusion and agricultural and hydrological applications of remote sensing.

Niko E. C. Verhoest received the engineering and the Ph.D. degrees in applied biological sciences from Ghent University, Ghent, Belgium, in 1994 and 2000, respectively.

He has been a Teaching Assistant (1998–2000) and an Assistant Professor (2000–2002) with the Laboratory of Hydrology and Water Management, Ghent University. In 2002, he became an Associate Professor in hydrology and water management, Faculty of Agricultural and Applied Biological Sciences, Ghent University. His research interests include hydrological applications of radar remote sensing.